Electronic Supplementary Material (ESI) for Environmental Science: Atmospheres.

Supplemental Information

Estimation of hourly black carbon aerosol concentrations from glass fiber filter tapes using image reflectance-based method

Abhishek Anand[1,2], Suryaprakash Kompalli[3], Eniola Ajiboye[3], Albert A. Presto[1,2*]

[1]Center for Atmospheric Particle Studies, Carnegie Mellon University, PA

[2]Department of Mechanical Engineering, Carnegie Mellon University, PA

[3]Carnegie Mellon University Africa, Rwanda

*Corresponding author: apresto@andrew.cmu.edu

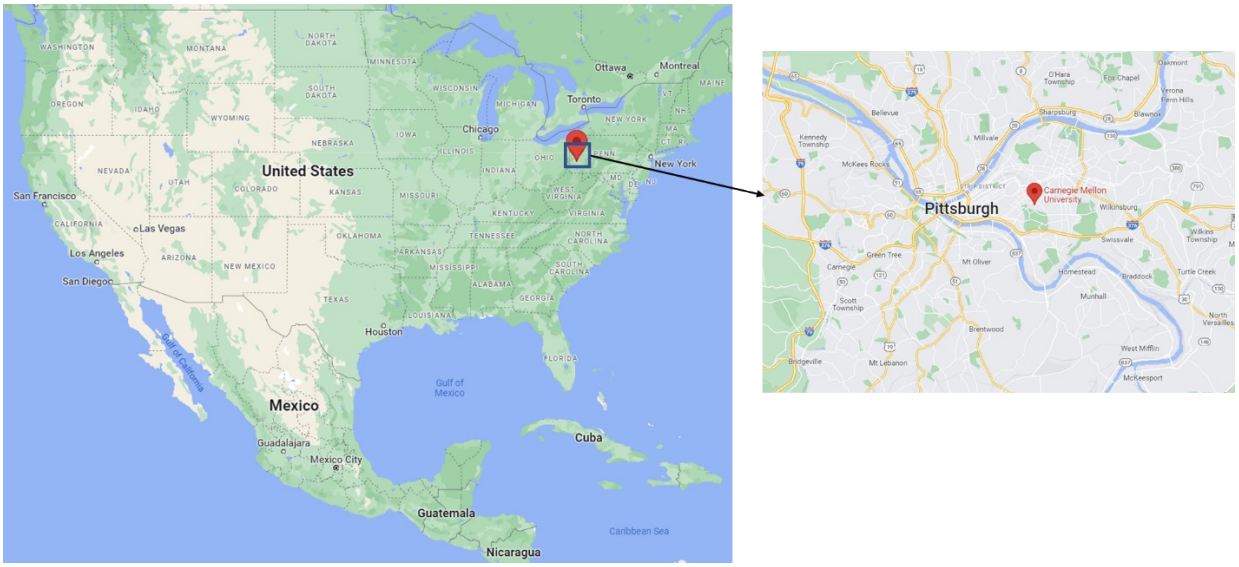

Figure S1: All ambient filter samples (51) were collected at Carnegie Mellon University in Pittsburgh, Pennsylvania (USA). The coordinates for the location are 40°26'33.4"N and 79°56'39.8"W.

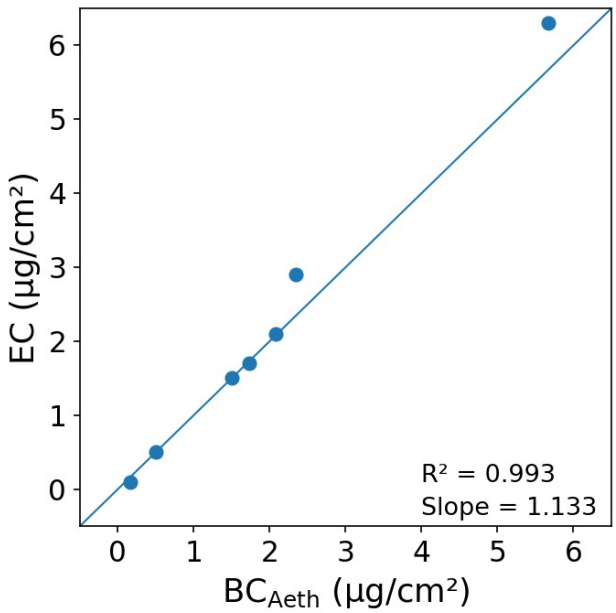

Figure S2: Comparison of two reference methods to measure black carbon (BC). EC represents thermo-optically estimated elemental carbon using IMPROVE-A, whereas BC_{Aeth} represents BC concentrations measured from an aethalometer (AE-31).

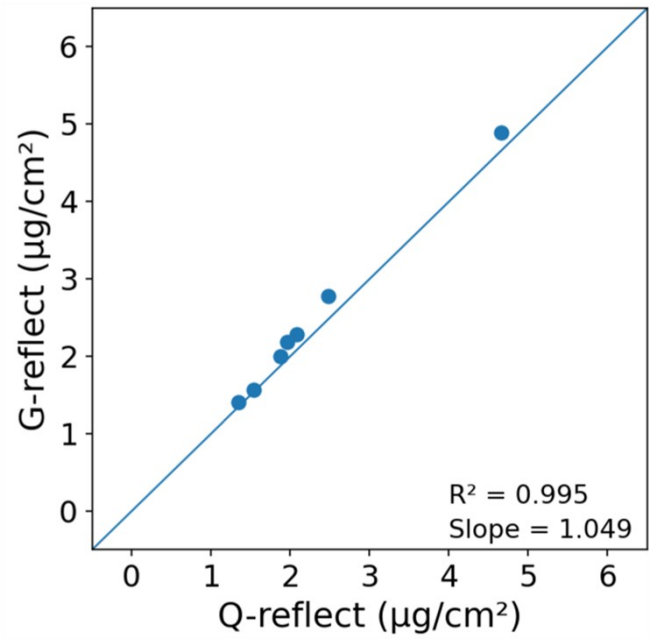

Figure S3: Comparison of performance of the image reflectance-based BC between glass (G-reflect) and quartz (Q-reflect) filters.

S1. Reference card details

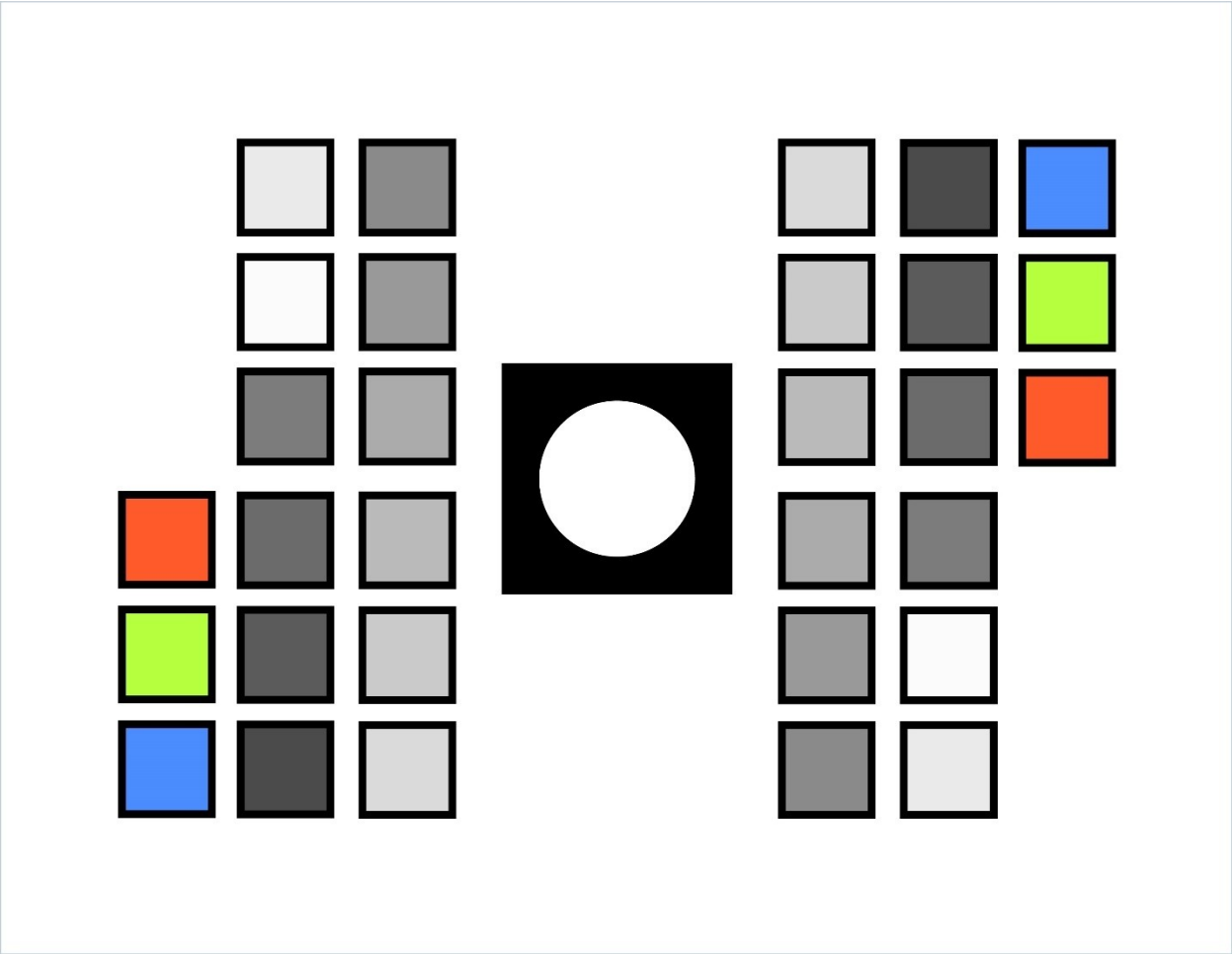

Figure S4: Reference card template (JPG file available)

The reference card is designed in Adobe Illustrator with RGB inputs for each of the squares on the template. The card is letter sized (8.5 x 11 inches) and is printed on a matte finish photo paper to avoid light reflections from the paper during photo capture. It is cost effective to use Photo Printing Services in FedEx or similar outlets, which also provides high quality prints. Any other color printer that can print a uniformly distributed color for the squares would work too.

S2. Effect of lighting conditions on estimation of BC concentrations

A uniform lighting is critical for image capturing to ensure same effect of color correction is applied for the entire reference card. Point sources such as LEDs might introduced localized errors during color correction. Therefore, we used two 6000 K ring lights to establish a uniform diffused lighting with capabilities with 10 different light intensities.

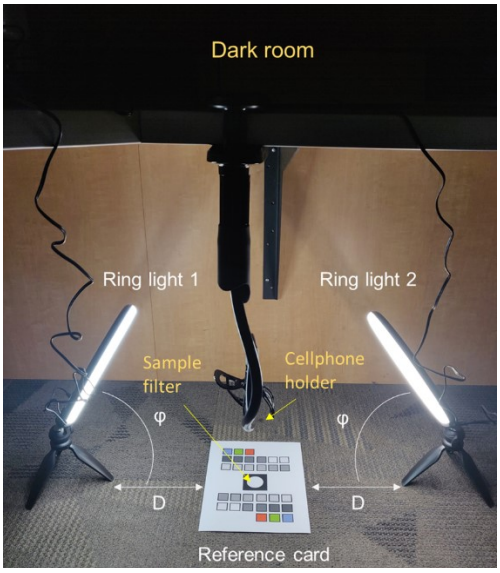

Figure S5: Image capturing setup that includes a pair of 6000K ring lights placed equidistant (D = 8 inches) from the reference cards to ensure a uniform diffused lighting environment. The lights were set at second maximum intensity (level 9). Ring lights were the only source of light in the room to avoid optical interference.

We selected two filter samples in different BC concentration ranges and varied the intensities of the lights simultaneously to study the effects of lighting variations on the performance of image reflectance method. The minimum light intensity was limited at level 6 as the lower levels were too diminished compared to usual working environments. Level 9 was used as a standard to compare the red scale change in filter samples. We observed a percentage red scale change of only

0.4% and 3.7% change in BC estimation for lower concentration sample (1.725 µg cm^{-2}), whereas only 1% change in R and a maximum change in BC of 3.8% for the higher BC sample (8.089 µg cm^{-2}).

Table S1: Effect of varying light intensities on RGB color channel and BC estimations of filter samples. The light intensities varied from level 6 to 10 for two samples with BC concentrations (C_A) of 1.725 µg cm^{-2} (Sample ID: 25) and 8.089 µg cm^{-2} (Sample ID: 21). The changes in R and BC are calculated with those in level 9 as a standard.

Sample ID	Light Intensity	R	G	B	%ΔR/R	%ΔBC/BC
25	6	224	220	203	0.4	-3.7
	7	224	220	203	0.4	-3.7
	8	224	220	204	0.4	-3.7
	9 (reference)	223	220	205	-	-
	10	223	220	206	0.0	0.0
21	6	172	167	148	1.2	-3.8
	7	171	167	149	0.6	-1.9
	8	171	167	149	0.6	-1.9
	9 (reference)	170	166	149	-	-
	10	171	167	152	0.6	-1.9

(a) (b)

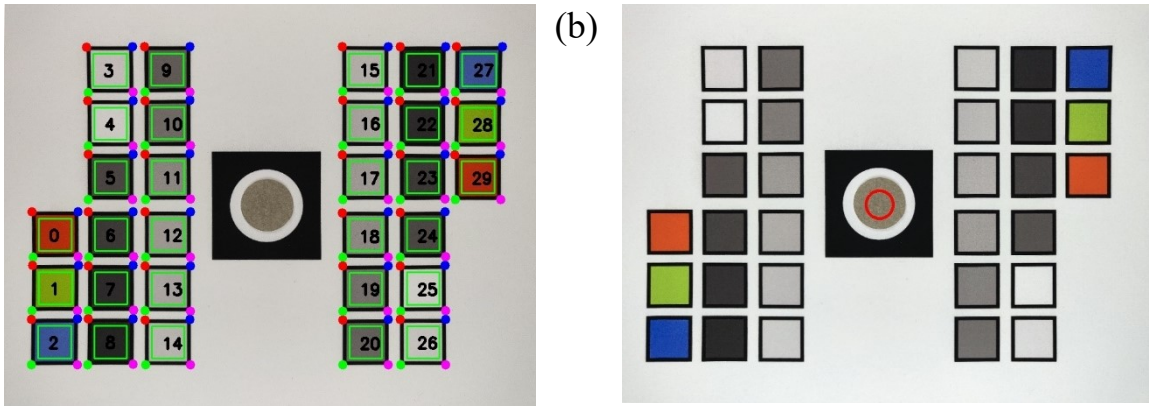

Figure S6: Intermediate stages of image processing for the filter sample and reference card assembly: (a) contour detection for the squares with predesignated RGB values, and (b) the red circle shows the portion of filter extracted for averaged RGB values for the sample. The extraction area can be varied as needed.

Table S2: RGB channels and reference BC area concentrations (C_A derived from BC_{Aeth}) are listed for the 51 ambient filter samples collected for model training.

Sample No.	**C_A (µg cm^{-2})**	**R**	**G**	**B**
1	0.163	248	214	189
2	0.499	244	246	244
3	2.088	217	214	200
4	1.511	230	228	214
5	2.355	208	201	179
6	5.675	173	166	140
7	1.740	224	221	207
8	1.678	223	221	207
9	9.077	145	139	112
10	4.329	206	200	176
11	6.623	171	166	144
12	3.761	200	198	177
13	8.227	170	162	133
14	7.553	164	160	137
15	15.432	130	127	107
16	5.451	189	185	165
17	3.628	202	201	186
18	6.320	175	170	151
19	0.816	240	241	234
20	7.294	168	163	140
21	8.089	170	166	149
22	8.794	163	160	141
23	5.144	200	198	189
24	8.095	169	163	149
25	1.725	223	220	205

26	1.335	234	232	222
27	0.928	238	239	233
28	7.801	172	165	133
29	2.847	213	210	188
30	15.482	123	120	96
31	9.976	140	137	114
32	0.874	236	238	230
33	3.311	199	194	175
34	1.880	220	220	208
35	9.921	154	148	125
36	3.597	206	204	187
37	3.905	198	195	180
38	4.507	193	189	169
39	4.763	195	192	180
40	5.262	188	185	171
41	1.043	216	215	210
42	2.025	196	193	184
43	4.844	167	160	146
44	1.294	231	229	217
45	0.667	240	241	237
46	0.464	247	248	246
47	3.900	207	203	178
48	1.424	233	233	218
49	4.988	174	170	148
50	4.538	187	182	154
51	2.165	219	226	212

S3. Defining R threshold for hybrid models

To achieve the optimum performance of a hybrid model, i.e., high R^2, low RMSE, and low MAE, we defined a threshold value of R (R_T). A hybrid model was comprised of separate functions for high BC concentrations ($R \leq R_T$) and lower BC concentrations ($R > R_T$). The threshold BC concentration is designated as B_{th}. We tried (a) getting a smooth transition at the threshold, i.e., the value of BC using both functions should be the same at R_T, (b) getting a BC value of 0 at R=255, and (c) minimizing overall R^2, MAE, and RMSE for the dataset. For example, the threshold for the exponential model is 224, which corresponds to 1.66 μg m^{-3}.

Table S3: Average daily EC from CSN (EC-CSN) and image reflectance-based BC (BC-OPT) for Lawrenceville and Liberty sites during the respective validation periods.

Site	**Date (mm/dd/yyyy)**	**EC-CSN (µg m^{-3})**	**BC-OPT (µg m^{-3})**
Liberty	3/16/2020	0.581	0.376
Liberty	3/22/2020	0.171	0.210
Liberty	3/28/2020	0.651	0.413
Liberty	4/3/2020	0.211	0.241
Liberty	4/9/2020	0.22	0.335
Liberty	4/15/2020	0.198	0.207
Liberty	4/21/2020	0.456	0.443
Liberty	4/27/2020	0.247	0.137
Liberty	5/3/2020	0.777	0.605
Liberty	5/9/2020	0.262	0.208
Liberty	5/15/2020	0.579	0.349
Liberty	5/21/2020	0.288	0.172
Liberty	5/27/2020	0.224	0.174
Lawrenceville	7/14/2020	0.384	0.608
Lawrenceville	7/17/2020	0.341	0.379
Lawrenceville	7/20/2020	0.209	0.566
Lawrenceville	7/23/2020	0.271	0.320
Lawrenceville	7/26/2020	0.594	0.235
Lawrenceville	7/29/2020	0.496	0.325
Lawrenceville	8/1/2020	0.472	0.513
Lawrenceville	8/4/2020	0.319	0.216
Lawrenceville	8/7/2020	0.385	0.236
Lawrenceville	8/10/2020	0.421	0.346
Lawrenceville	8/13/2020	0.326	0.472
Lawrenceville	8/16/2020	0.28	0.260

Lawrenceville	8/19/2020	0.241	0.236
Lawrenceville	8/22/2020	0.586	0.262
Lawrenceville	8/25/2020	0.317	0.276
Lawrenceville	8/28/2020	0.315	0.410
Lawrenceville	8/31/2020	0.395	0.146
Lawrenceville	9/3/2020	0.432	0.283
Lawrenceville	9/6/2020	0.326	0.542

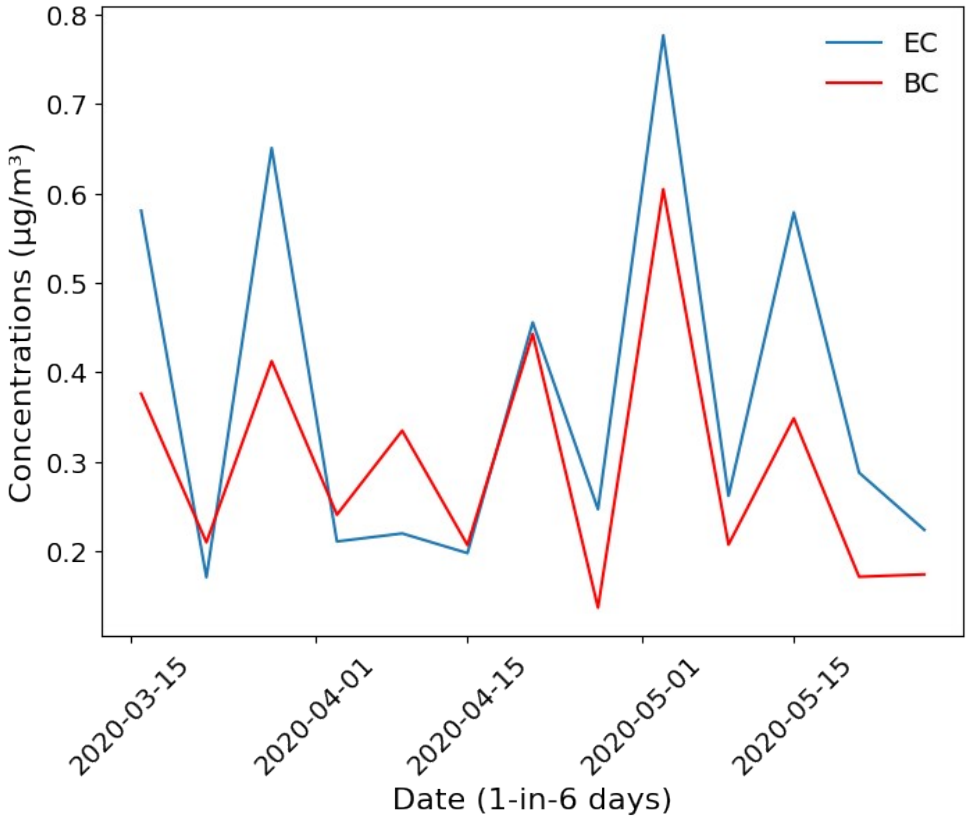

Figure S7: Time series of average daily EC from CSN (EC-CSN) and image reflectance-based BC (BC-OPT) for Liberty sites during the validation period.

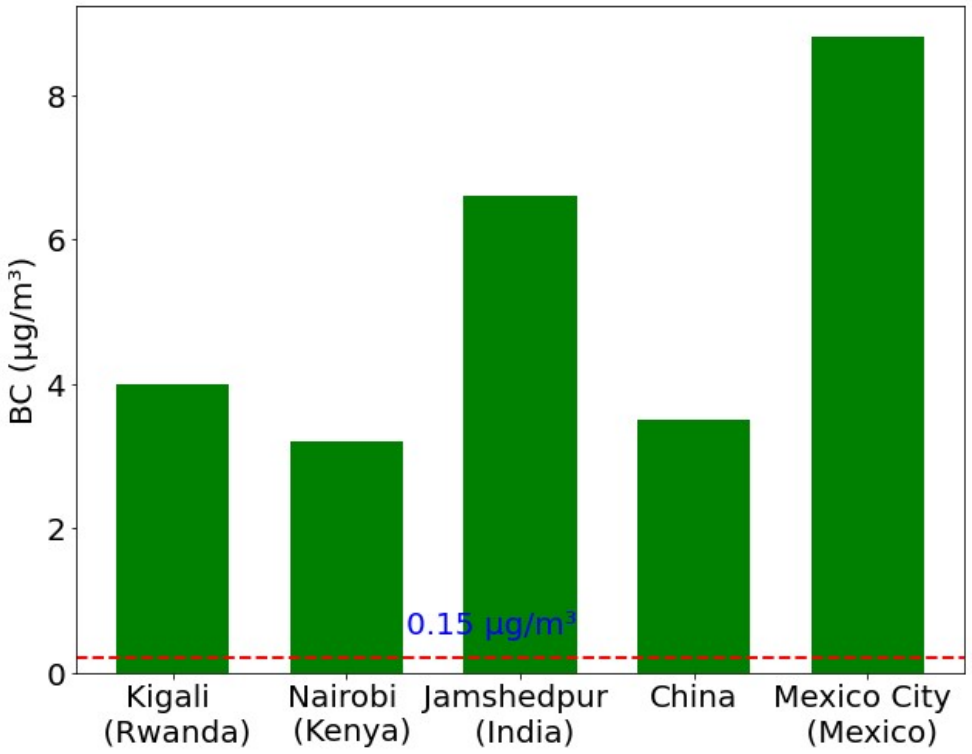

Figure S8: Bar charts showing annual mean concentrations for countries in the Global South. The dashed horizontal line represents the hourly effective detection limit for the image-based BC estimation method. The concentrations are approximately 20-60 times of the EDL.[1–6]

S4. Wood smoke sampling

The samples collected in 2004 were from burning mixed wood types (oak, cherry, and some ash).[7] An EPA-approved wood stove (602 EB Classic, Jøtul AS) was used for combustion. We used the same stove for sampling 2022 wood smoke and wood smoke deposited on ambient samples. Figure S7 shows the sampling setup. The combustion emission temperature was between 130-150 ℃. The exhaust was diluted with a diluter (Dekati® Diluter DI-1000, Dekati Ltd, Finland) by mixing clean heated air (130-150 ℃) with the exhaust to avoid condensation on smoke particles. A pressurized air heater (H41, Dekati Ltd, Finland) was used to heat and maintain the temperature. The diluted emission was sent to a large PTFE chamber (~ 3m × 3m) for further dilution and mixing. The well-mixed wood smoke was sampled to glass-fiber filters at 1 m^3 h^{-1} for varied intervals to deposit different BC loadings.

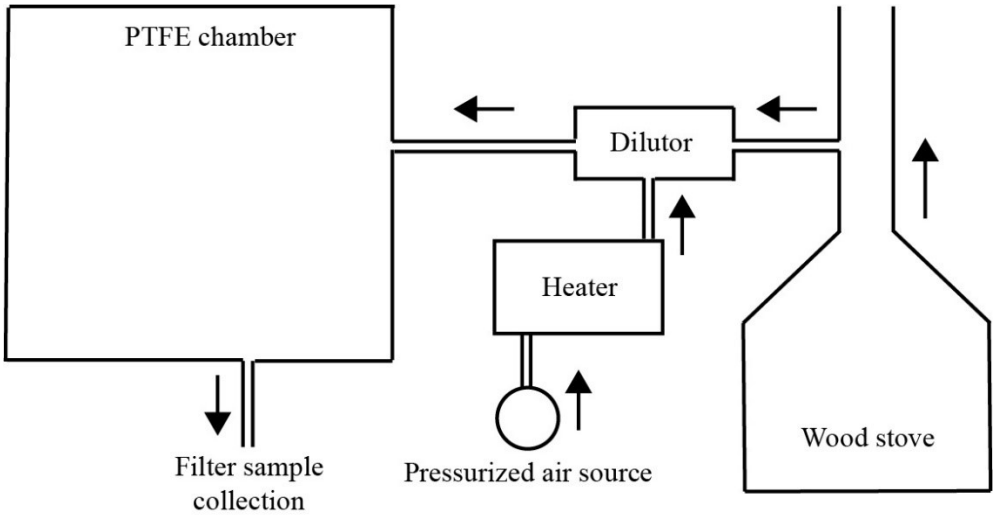

Figure S9: Setup to sample wood combustion smoke on filters.

Table S4: RGB channels are listed for the 156 filter samples collected for wood smoke-sample detection analysis.

Sample No.	**Source**	**R**	**G**	**B**
1	Ambient	248	214	189
2	Ambient	244	246	244
3	Ambient	217	214	200
4	Ambient	230	228	214
5	Ambient	208	201	179
6	Ambient	173	166	140
7	Ambient	224	221	207
8	Ambient	223	221	207
9	Ambient	145	139	112
10	Ambient	206	200	176
11	Ambient	171	166	144
12	Ambient	200	198	177
13	Ambient	170	162	133
14	Ambient	164	160	137
15	Ambient	130	127	107
16	Ambient	189	185	165
17	Ambient	202	201	186
18	Ambient	175	170	151
19	Ambient	240	241	234
20	Ambient	168	163	140
21	Ambient	170	166	149
22	Ambient	163	160	141
23	Ambient	200	198	189
24	Ambient	169	163	149
25	Ambient	223	220	205

26	Ambient	234	232	222
27	Ambient	238	239	233
28	Ambient	172	165	133
29	Ambient	213	210	188
30	Ambient	123	120	96
31	Ambient	140	137	114
32	Ambient	236	238	230
33	Ambient	199	194	175
34	Ambient	220	220	208
35	Ambient	154	148	125
36	Ambient	206	204	187
37	Ambient	198	195	180
38	Ambient	193	189	169
39	Ambient	195	192	180
40	Ambient	188	185	171
41	Ambient	216	215	210
42	Ambient	196	193	184
43	Ambient	167	160	146
44	Ambient	231	229	217
45	Ambient	240	241	237
46	Ambient	247	248	246
47	Ambient	207	203	178
48	Ambient	233	233	218
49	Ambient	174	170	148
50	Ambient	187	182	154
51	Ambient	219	226	212
52	Diesel	128	120	105
53	Diesel	134	131	120
54	Diesel	94	86	75

55	Diesel	35	34	33
56	Diesel	127	118	104
57	Diesel	94	86	75
58	Diesel	102	94	84
59	Diesel	132	122	101
60	Diesel	24	25	28
61	Diesel	107	96	82
62	Diesel	126	119	105
63	Diesel	29	29	30
64	Diesel	124	117	104
65	Diesel	151	144	130
66	Diesel	73	69	66
67	Diesel	62	60	57
68	Diesel	131	125	112
69	Wood smoke 2004	140	99	36
70	Wood smoke 2004	154	115	42
71	Wood smoke 2004	200	190	151
72	Wood smoke 2004	179	158	94
73	Wood smoke 2004	187	159	76
74	Wood smoke 2004	212	207	192
75	Wood smoke 2004	131	94	38
76	Wood smoke 2004	188	168	106
77	Wood smoke 2004	168	141	80
78	Wood smoke 2004	100	83	55
79	Wood smoke 2004	138	111	65
80	Wood smoke 2004	149	120	64
81	Wood smoke 2004	132	104	52
82	Wood smoke 2004	167	150	109
83	Wood smoke 2004	128	101	50

84	Wood smoke 2004	182	169	143
85	Wood smoke 2004	79	56	38
86	Wood smoke 2004	170	154	116
87	Wood smoke 2004	79	64	44
88	Wood smoke 2004	192	174	131
89	Wood smoke 2004	190	170	121
90	Wood smoke 2004	168	157	135
91	Wood smoke 2004	122	102	68
92	Wood smoke 2004	194	176	132
93	Wood smoke 2004	187	181	163
94	Wood smoke 2004	186	179	160
95	Wood smoke 2022	214	208	187
96	Wood smoke 2022	199	194	177
97	Wood smoke 2022	199	196	183
98	Wood smoke 2022	106	95	76
99	Wood smoke 2022	153	142	119
100	Wood smoke 2022	69	60	48
101	Wood smoke 2022	170	161	140
102	Wood smoke 2022	220	219	214
103	Wood smoke 2022	214	214	204
104	Wood smoke 2022	219	220	211
105	Wood smoke 2022	218	216	205
106	Wood smoke 2022	231	232	230
107	Wood smoke 2022	228	228	223
108	Wood smoke 2022	224	225	219
109	Wood smoke 2022	225	225	218
110	Wood smoke 2022	220	219	206
111	Wood smoke 2022	198	192	172
112	Wood smoke 2022	185	176	155

113	Wood smoke 2022	207	203	188
114	Wood smoke 2022	209	206	192
115	Wood smoke 2022	205	201	185
116	Wood smoke 2022	181	173	152
117	Wood smoke 2022	179	170	146
118	Wood smoke 2022	161	149	123
119	Wood smoke 2022	152	141	120
120	Wood smoke 2022	142	132	110
121	Wood smoke 2022	212	209	195
122	Wood smoke 2022	202	194	171
123	Wood smoke 2022	206	200	177
124	Wood smoke 2022	195	187	163
125	Wood smoke 2022	164	154	132
126	Wood smoke 2022	158	147	124
127	Wood smoke 2022	168	158	136
128	Wood smoke 2022	177	168	146
129	Wood smoke 2022	174	165	143
130	Ambient + wood smoke	220	220	213
131	Ambient + wood smoke	216	217	208
132	Ambient + wood smoke	179	172	151
133	Ambient + wood smoke	192	186	168
134	Ambient + wood smoke	168	158	134
135	Ambient + wood smoke	189	183	165
136	Ambient + wood smoke	195	188	170
137	Ambient + wood smoke	193	186	167
138	Ambient + wood smoke	209	206	194
139	Ambient + wood smoke	207	204	193
140	Ambient + wood smoke	198	193	177
141	Ambient + wood smoke	195	189	171

142	Ambient + wood smoke	204	202	190
143	Ambient + wood smoke	217	216	206
144	Ambient + wood smoke	155	145	125
145	Ambient + wood smoke	183	177	161
146	Ambient + wood smoke	153	143	121
147	Ambient + wood smoke	161	151	131
148	Ambient + wood smoke	151	141	118
149	Ambient + wood smoke	170	162	143
150	Ambient + wood smoke	179	170	151
151	Ambient + wood smoke	175	167	148
152	Ambient + wood smoke	191	186	172
153	Ambient + wood smoke	185	180	164
154	Ambient + wood smoke	169	160	140
155	Ambient + wood smoke	170	161	140
156	Ambient + wood smoke	186	180	162

References

(1) Zhang, Y.; Li, Y.; Guo, J.; Wang, Y.; Chen, D.; Chen, H. The Climatology and Trend of Black Carbon in China from 12-Year Ground Observations. *Clim. Dyn.* **2019**, *53* (9–10), 5881–5892. https://doi.org/10.1007/S00382-019-04903-0/FIGURES/9.

(2) Subramanian, R.; Kagabo, A. S.; Baharane, V.; Guhirwa, S.; Sindayigaya, C.; Malings, C.; Williams, N. J.; Kalisa, E.; Li, H.; Adams, P.; Robinson, A. L.; DeWitt, H. L.; Gasore, J.; Jaramillo, P. Air Pollution in Kigali, Rwanda: Spatial and Temporal Variability, Source Contributions, and the Impact of Car-Free Sundays. *Clean Air J.* **2020**, *30* (2). https://doi.org/10.17159/CAJ/2020/30/2.8023.

(3) Langley Dewitt, H.; Gasore, J.; Rupakheti, M.; Potter, K. E.; Prinn, R. G.; De Dieu Ndikubwimana, J.; Nkusi, J.; Safari, B. Seasonal and Diurnal Variability in O3, Black Carbon, and CO Measured at the Rwanda Climate Observatory. *Atmos. Chem. Phys.* **2019**, *19* (3), 2063–2078. https://doi.org/10.5194/acp-19-2063-2019.

(4) Gatari, M. J.; Kinney, P. L.; Yan, B.; Sclar, E.; Volavka-Close, N.; Ngo, N. S.; Mwaniki Gaita, S.; Law, A.; Ndiba, P. K.; Gachanja, A.; Graeff, J.; Chillrud, S. N. High Airborne Black Carbon Concentrations Measured near Roadways in Nairobi, Kenya. *Transp. Res. Part D Transp. Environ.* **2019**, *68*, 99–109. https://doi.org/10.1016/J.TRD.2017.10.002.

(5) Ambade, B.; Sankar, T. K.; Panicker, A. S.; Gautam, A. S.; Gautam, S. Characterization, Seasonal Variation, Source Apportionment and Health Risk Assessment of Black Carbon over an Urban Region of East India. *Urban Clim.* **2021**, *38*, 100896. https://doi.org/10.1016/J.UCLIM.2021.100896.

(6) Retama, A.; Baumgardner, D.; Raga, G. B.; McMeeking, G. R.; Walker, J. W. Seasonal and

Diurnal Trends in Black Carbon Properties and Co-Pollutants in Mexico City. *Atmos. Chem. Phys.* **2015**, *15* (16), 9693–9709. https://doi.org/10.5194/ACP-15-9693-2015.

(7) Lipsky, E. M.; Robinson, A. L. Effects of Dilution on Fine Particle Mass and Partitioning of Semivolatile Organics in Diesel Exhaust and Wood Smoke. *Environ. Sci. Technol.* **2006**, *40* (1), 155–162. https://doi.org/10.1021/ES050319P/ASSET/IMAGES/MEDIUM/ES050319PE00003.GIF.